Journal of Materials Chemistry

Cite this: J. Mater. Chem., 2012, 22, 11146

www.rsc.org/materials

PAPER

High pseudocapacitance material prepared *via in situ* growth of $Ni(OH)_2$ nanoflakes on reduced graphene oxide†

Jie Chang, Huan Xu, Jing Sun* and Lian Gao

Received 13th January 2012, Accepted 27th March 2012
DOI: 10.1039/c2jm30243h

We report a two step approach to fabricate reduced graphene oxide/nickel oxide (RGO/$Ni(OH)_2$) nanocomposites by combining the reduction of graphene oxide (GO) with the help of PVP and the subsequent hydrolysis of $Ni(Ac)_2$ on RGO. The nanocomposites were characterized by transmission electron microscopy (TEM), scanning electron microscopy (SEM), Raman spectra, X-ray power diffraction (XRD) and thermogravimetry (TG). The results show that $Ni(OH)_2$ nanoflakes with lateral sizes of tens of nm and thicknesses of several nm were homogeneously attached on the surface of RGO. Cyclic voltammetry (CV) and galvanostatic charge and discharge tests were conducted to study the performance of RGO/$Ni(OH)_2$. The RGO/$Ni(OH)_2$ composites demonstrate much better capacitance performance and rate performance compared with pure $Ni(OH)_2$ due to synergetic effects. The hybrid material with 84.5 wt% $Ni(OH)_2$ presents an extremely high specific capacitance of 1828 F g^{-1} at 1 A g^{-1} and an energy density of 63.5 Wh kg^{-1} at a power density of 250 W kg^{-1}. The corresponding values at 10 A g^{-1} are 780 F g^{-1}, 27.1 Wh kg^{-1} and 2500 W kg^{-1}. The specific capacitance can maintain at a high value of 840 F g^{-1} after 1000 charge and discharge cycles at 6 A g^{-1}.

Introduction

As one of the highly promising auxiliaries or candidates for lithium ion batteries, electrochemical supercapacitors have drawn increasing attention in recent years. Among various energy storage devices, supercapacitors possess extreme high power density, moderate energy density and long cycle life.[1,2] Traditional pseudocapacitance materials can be divided mainly into two categories, transition-metal oxides[3–8] (or hydroxides)[9,10] and conductive polymers,[11–13] the specific capacitances of which are still far from their theoretical values. A lot of effort has been devoted to the enhancement of their specific capacitance and energy density. As the Faradic redox reaction occurs only on the surface and near the surface of the electrode, the remaining part of the pseudocapacitance material not only has no contribution to the redox reaction but also hampers electron and ion transport due to its poor conductivity. Hence, the full utilization of pseudocapacitance materials has become a most pressing problem.

Incorporating active materials with carbonaceous nanomaterials such as activated carbon,[14] carbon nanotubes[15,16] and graphene[17–21] is usually adopted because of their large surface area and high conductivity. Reduced graphene oxide (RGO) is an ideal hybrid material due to its 2-D planar structure, easy functionality resulting from the residual oxygen containing groups on the surface, as well as the low cost compared with carbon nanotubes.[22–25] Recently, a lot of work has been reported on RGO composite supercapacitors, especially the RGO based transition-metal oxides or hydroxides (NiO,[18] $Ni(OH)_2$,[19,26] Fe_3O_4,[20,21] *et al.*), which can provide a large specific capacitance due to multi electron transfer during Faradaic reactions. Nevertheless, the real specific capacitance calculated for the whole mass of hybrid materials (not only based on the mass of pseudocapacitance materials attached on the surface of graphene) is still very low. There are two main reasons for the low real capacitance. Firstly, the graphene obtained from the reduction of graphene oxide (GO) is usually stacked with each other, which dramatically reduces its surface area. Secondly, applying a large amount of graphene can improve the performance of a small amount of pseudocapacitance material, though there is no doubt that the theoretical specific capacitance of the whole hybrid material will be decreased. Hence, it is necessary to balance the ratio between RGO and the pseudocapacitance materials to make full use of their synergetic effect.

Herein, we report a facile approach to *in situ* synthesize $Ni(OH)_2$ nanoflakes on polyvinylpyrrolidone (PVP) dispersed RGO. The RGO/$Ni(OH)_2$ (with 84.5 wt% of $Ni(OH)_2$) exhibits an extremely high energy density, better rate performance and cycling stability, which makes it a promising electrode material for future energy storage systems.

The State Key Lab of High Performance Ceramics and Superfine Microstructure, Shanghai Institute of Ceramics, Chinese Academy of Sciences, 1295 Ding Xi Road, Shanghai 200050, China. E-mail: jingsun@mail.sic.ac.cn; Fax: +86 21 52413122; Tel: + 86 21 52414301

† Electronic supplementary information (ESI) available: TG curves of RGO/$Ni(OH)_2$ with various mass ratio of $Ni(Ac)_2 \cdot 4H_2O$ to GO. Typical morphology of RGO/$Ni(OH)_2$ and pure $Ni(OH)_2$. See DOI: 10.1039/c2jm30243h

Experimental

GO preparation

All the chemicals are of analytical grade and were used without further purification. GO was made from natural graphite *via* a modified Hummers method previously reported by our group.[27] In a typical synthesis, 1 g graphite powder and 1 g sodium nitrate were added into 46 mL of 98% H_2SO_4 solution in an ice bath. After constant stirring for 4 h, 6 g $KMnO_4$ was added. After stirring for 3 days, 50 mL distilled water and 10 mL of 30% H_2O_2 solution were dropped into the mixture. To purify the graphene oxide, the mixture was centrifuged, and subsequent washed with 10% HCl solution and distilled water.

Synthesis of PVP dispersed graphene

Typically, 50 mg GO was distributed in 50 mL distilled water to obtain a homogeneous stable brown dispersion with the aid of ultrasonication. Then the mixture was maintained in a 50 °C bath for 8 h followed by the addition of 50 mL of 2 g L^{-1} PVP (K30) solution under stirring. Finally, the mixture was reduced with hydrazine (100 μL) at 95 °C for 1 h.

Preparation of $Ni(OH)_2$/RGO nanocomposites

For the synthesis of RGO/$Ni(OH)_2$ (with 84.5 wt% $Ni(OH)_2$), 1.68 g $Ni(AC)_2 \cdot 4H_2O$ was added into 100 mL of the as-prepared PVP-RGO solution. Then the mixture was refluxed at 100 °C for 4 h under stirring. The precipitates were collected through a filtration, washing and drying process. Finally, the composites were annealed for 6 h at 200 °C under air atmosphere. For comparison, pure $Ni(OH)_2$ was also prepared using a similar method except for the addition of GO.

Characterization

Powder X-ray diffraction (XRD) analyses were performed on a Bruker D8 Advance diffractometer with Cu radiation at $\lambda = 0.15418$ nm. Thermogravimetric analyses (TG) were run on a STA449C thermogravimetric analyzer from 0 °C to 800 °C. Raman spectra were recorded on a DXR Raman Microscope with an excitation wavelength of 532 nm. The morphology was observed on a transmission electron microscope (TEM JEOL JEM-2100F) and a scanning electron microscope (SEM JEOL S-4800). To measure the sheet resistance, the powders were mechanically compacted to produce thin disks. Then the disks were measured at room temperature by means of an Accent HL 5500.

Electrochemical measurement

The electrochemical properties of the products were investigated under a three electrode system. A HgO/Hg electrode filled with 1 M NaOH was used as the reference electrode, platinum wire was used as the counter electrode, and 1 M KOH was used as the electrolyte. The working electrodes were fabricated by mixing the prepared powders with 20 wt% acetylene black and 10 wt% polyvinylidene fluoride (PVDF) with the addition of a little ethanol. Then the mixture was dried at 60 °C overnight. 4 mg of the prepared mixture was pressed onto nickel foam (1.5 cm × 1.5 cm) to make electrodes. Before the test, the working electrode was soaked in 1 M KOH for 2 h.

The cyclic voltammograms (CV) were recorded on a CHI 660D electrochemistry workstation. The galvanostatic charge and discharge tests were carried out on a LAND CT2001A cell measurement system. The specific capacitance, energy density and power density were calculated from discharging curves using the following equations:

$$C_s = \frac{It}{m\Delta V}$$

$$E = \frac{1}{2} C_s (\Delta V)^2$$

$$P = \frac{E}{t}$$

where C_s represents the specific capacitance, I is the discharge current, t is the time for a full discharge, m indicates the mass of active materials, ΔV is the potential range of a full discharge, E is the energy density and P is the power density.

Results and discussion

GO used in this work was produced from graphite using the modified Hummers method. The reduction of GO with hydrazine was conducted in the presence of PVP, and the obtained mixture can remain stable for a couple of months. Moreover, RGO could be easily redispersed in water after a filtering, washing and drying process. TEM images give the representative morphology of the GO (Fig. 1a) and RGO (Fig. 1b). The GO exhibits some wrinkles on the surface revealing its thin thickness, and the lateral size is several millimeters. After reduction, the morphology does not change obviously. The digital pictures (inset in Fig. 1) display the GO and RGO at a concentration of 1 g L^{-1} after settling for 2 months which clearly demonstrate their stability. Estimated from the XPS results, the ratio of C to O climbs from 2 to 5.4 indicating that considerable deoxygenation was caused during the reduction process.

The Raman spectra (see Fig. 2) of GO and RGO are characterized by two main features, the G band (~1589 cm^{-1}) representing the in-plane bond-stretching motion of the pairs of C sp^2 atoms and the D band (~1347 cm^{-1}) corresponding to the

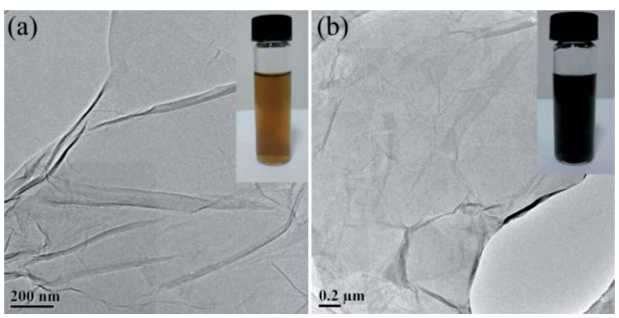

Fig. 1 Representative TEM images of GO (a) and RGO (b), the insets are the digital images of GO and RGO at a concentration of 1 g L^{-1}.

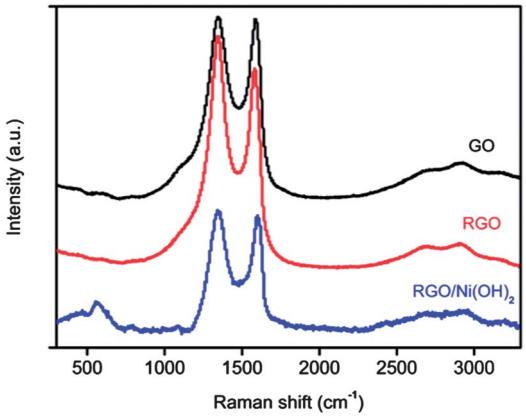

Fig. 2 Raman spectra patterns of GO, RGO and RGO/$Ni(OH)_2$ nanocomposites with 84.5 wt% $Ni(OH)_2$.

breathing modes of rings or K-point phonons of A_{1g} symmetry. We also calculated the area ratio of the D band to the G band, the results show that after reduction the ratio increases from 1.33 to 1.57 indicating a decrease in the size of the in-plane sp^2 domains which is very close to the previous report. The peak located at 570 cm^{-1} in the RGO/$Ni(OH)_2$ pattern can be attributed to $Ni(OH)_2$.[17]

Fig. 3 shows the XRD patterns of the as-prepared pure $Ni(OH)_2$ and hybrid RGO/$Ni(OH)_2$ materials. For the XRD patterns of $Ni(OH)_2$, all the peaks can be indexed to hexagonal nickel hydroxide (PDF#14-0117). For the RGO/$Ni(OH)_2$ nanocomposites, the (001) peak at a 2θ value of 19° differentiates into two peaks, and the reason is still obscure. The weight percentage of $Ni(OH)_2$ in the composites was estimated by thermogravimetry (TG) in air. The residues were all NiO when the composites were heated to 800 °C, based on which we calculated that the weight percent of $Ni(OH)_2$ was 84.5% with the precursor mass ratio $Ni(Ac)_2 \cdot 4H_2O$ to GO of 33.6 : 1 (see Fig. S1†). The XRD pattern of RGO shows a broad diffraction peak at ~25° which is very close to that of pristine graphite implying that GO is readily reduced.

SEM and TEM images (see Fig. 4) show the typical morphology and crystallinity of the RGO/$Ni(OH)_2$ nanocomposites. From the TEM images, it can be seen that graphene is coated with thin $Ni(OH)_2$ nanoflakes with lateral sizes of tens

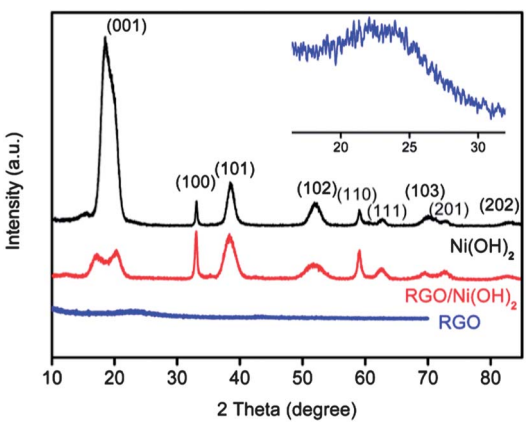

Fig. 3 XRD patterns of RGO, RGO/$Ni(OH)_2$ (with 84.5 wt% $Ni(OH)_2$) and pure $Ni(OH)_2$ (inset is the magnified view of RGO).

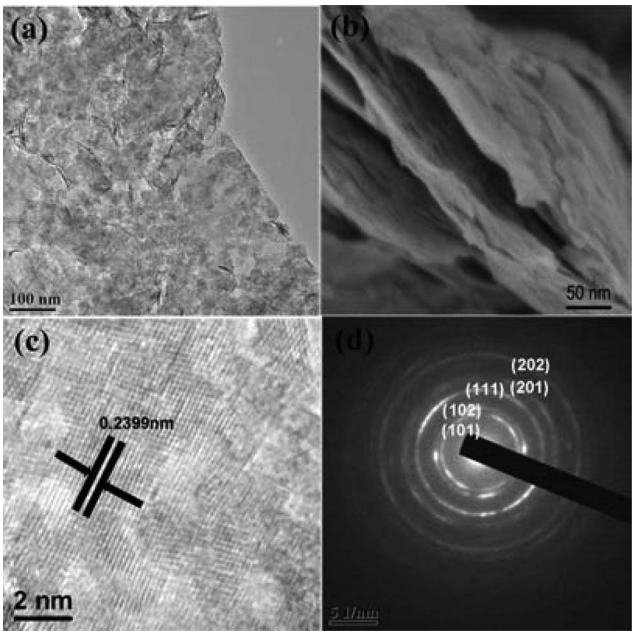

Fig. 4 Typical morphology of RGO/$Ni(OH)_2$ with 84.5 wt% $Ni(OH)_2$, TEM image (a), SEM image (b), HRTEM image (c) and SAED (d).

of nm. From the SEM images, layered graphene is still faintly visible surrounded by $Ni(OH)_2$, and the thickness of the RGO/$Ni(OH)_2$ is about 10–20 nm. The high resolution TEM image manifests that the lattice fringe of the $Ni(OH)_2$ is 0.2399 nm, corresponding to the (101) plane of $Ni(OH)_2$. Besides, the selected area electronic diffraction pattern (SAED) shows well defined rings, revealing the $Ni(OH)_2$ nanoflakes on RGO with a polycrystalline nature. The rings can be indexed to hexagonal nickel hydroxide which corresponds with the XRD results. The electrochemical performances of the composites were investigated by cyclic voltammetry and galvanostatic charge and discharge measurements.

The CV curves of pure $Ni(OH)_2$ and RGO/$Ni(OH)_2$ (see Fig. 5a) were recorded within the potential window of 0–0.7 V at a scan rate of 10 mV s^{-1} using a three electrode cell. Both the CV curves clearly exhibit a pair of cathodic and anodic peaks which correspond to the reversible reactions of $Ni(OH)_2$/NiOOH. The CV curve of RGO show a pair of redox peaks with low intensity which probably results from the oxidation of Ni foam in KOH solution. Generally, the specific capacitance of the electrode is directly proportional to its CV area. From the CV curves, we can easily figure out that the capacitance performance of $Ni(OH)_2$ is considerably enhanced when RGO is introduced.

To discuss in detail, galvanostatic charge and discharge measurements were carried out to study the capacitance performance and rate performance of $Ni(OH)_2$ and RGO/$Ni(OH)_2$. The galvanostatic discharge curves performed in a potential window of 0.05 V–0.55 V at various current densities are given in Fig. 5(b,c), based on which the specific capacitance were calculated. As illustrated in Fig. 5d, RGO/$Ni(OH)_2$ shows a much better capacitance performance compared with pure $Ni(OH)_2$ at all current densities. RGO/$Ni(OH)_2$ presents the highest specific capacitance of 1828 F g^{-1} at 1 A g^{-1}, then the value gradually decreases to 1680, 1376, 1092, 876 and 780 F g^{-1} when the current

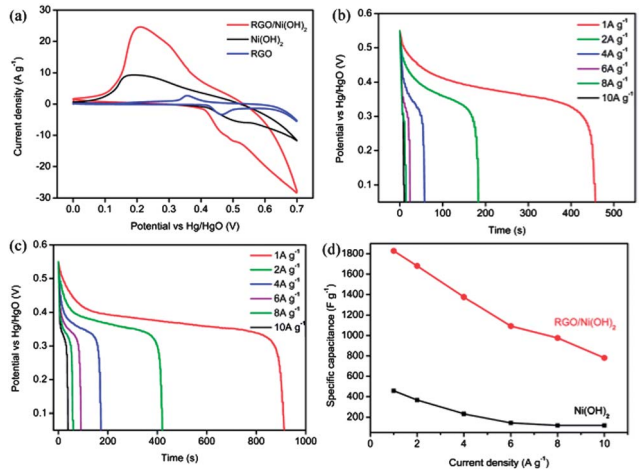

Fig. 5 CV curves of RGO, RGO/$Ni(OH)_2$ (with 84.5 wt% $Ni(OH)_2$) and $Ni(OH)_2$ recorded at a scan rate of 10 mV s^{-1} in the potential range of 0–0.7 V (a), discharge curves of pure $Ni(OH)_2$ (b) and RGO/$Ni(OH)_2$ (with 84.5 wt% $Ni(OH)_2$) (c) recorded at various current densities within a potential window of 0–0.55 V. Specific capacitance comparison between RGO/$Ni(OH)_2$ and $Ni(OH)_2$, (d). All data were taken in a three electrode cell in 1 M KOH using a HgO/Hg electrode and Pt wire as reference electrode and counter electrode, respectively.

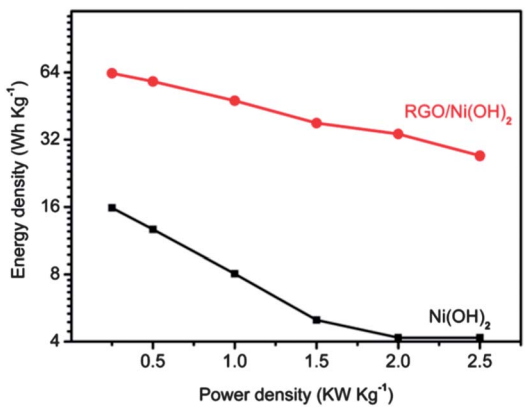

Fig. 6 Ragone plots of RGO/$Ni(OH)_2$ (with 84.5 wt% $Ni(OH)_2$) and $Ni(OH)_2$, the energy and power densities were derived from discharge curves at various current densities.

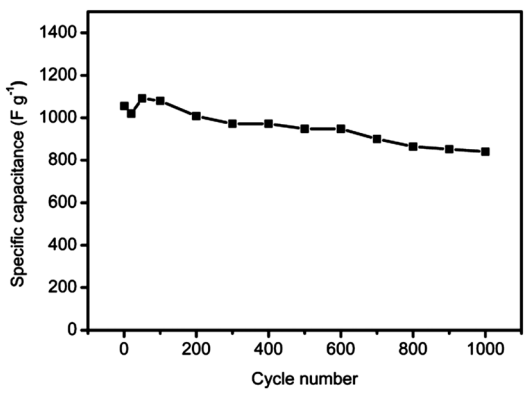

Fig. 7 Cyclic performance of RGO/$Ni(OH)_2$ (with 84.5 wt% $Ni(OH)_2$) nanocomposites at 6 A g^{-1}.

density increases to 2, 4, 6, 8 and 10 A g^{-1}, respectively. For pure $Ni(OH)_2$, the corresponding value is 457, 366, 232, 144, 120 and 120 F g^{-1} for 1, 2, 4, 6, 8 and 10 A g^{-1}, respectively. It is worth noting that the specific capacitance was calculated based on the total mass of RGO and $Ni(OH)_2$. If only based on the weight of $Ni(OH)_2$, we can obtain a rough value of 2147 F g^{-1} at 1 A g^{-1} (after excluding the pseudocapacitance contribution of residual functional groups on RGO and the double layer capacitance contribution of RGO ~87.8 F g^{-1}) which is very close to its theoretical pseudocapacitance value of 2074 F g^{-1}. This value is higher than the previous results using materials such as $Ni(OH)_2$ or RGO/$Ni(OH)_2$ nanocomposites as pseudocapacitance materials, such as 400 F g^{-1} for graphene/porous NiO,[18] 1335 F g^{-1} for $Ni(OH)_2$ nanoplates grown on graphene,[19] 1760.72 F g^{-1} for spherical $Ni(OH)_2$ grown on graphene,[26] 1025 F g^{-1} for porous NiO,[4] 781.5 F g^{-1} for graphene/Ni/Al double hydroxide,[17] *etc.* Notably, the rate performance of $Ni(OH)_2$ is largely improved after the introduction of RGO. There are two main reasons for the better capacitance and rate performances of RGO/$Ni(OH)_2$. Firstly, most of the $Ni(OH)_2$ nanoflakes attach tightly on the surface of RGO *via* either chemical covalent bonding or van der Waals interactions. The RGO could provide facile electron transport paths for the fast Faradaic reaction which is the key to both the higher specific capacitance and better rate performance. The sheet resistance was decreased from larger than 100 GΩ m^{-2} to 7.515 × 10^{10} Ω m^{-2} after the addition of RGO. Secondly, the addition of RGO could dramatically decrease the aggregation of the $Ni(OH)_2$ nanoflakes (see Fig. S2†), thus enhance the effective contacts between the active materials and the conductive agents.

To investigate the influence of the $Ni(OH)_2$ weight ratio on the electrochemical performance of the hybrid materials, the RGO/$Ni(OH)_2$ synthesized with different precursor mass ratios of $Ni(Ac)_2 \cdot 4H_2O$ to GO (6.7 : 1, 16.8 : 1, 33.6 : 1) was compared; the contents of $Ni(OH)_2$ were 61.1%, 78.2% and 84.5%, respectively (see Fig. S1 and S2†). The results indicate that the specific capacitance decreases with the increase of RGO (1828, 980 to 248 F g^{-1} at 1 A g^{-1}), while the rate performance is greatly enhanced (42.7%, 67.3% to 96.7% capacitance retention at 10 A g^{-1} in contrast with 1 A g^{-1}). The synergetic effect between RGO and $Ni(OH)_2$ may be responsible for the better capacitance retention rate at high current density.

Fig. 6 gives the Ragone plots of RGO/$Ni(OH)_2$ (with 84.5 wt% $Ni(OH)_2$) and $Ni(OH)_2$ calculated from discharge curves recorded at different current densities. For RGO/$Ni(OH)_2$, the energy density decreases gradually as the power density increases. It could deliver a high energy density of 63.5 Wh kg^{-1} at a power density of 250 W kg^{-1}, and still can maintains a high value of 27.1 Wh kg^{-1} at 2500 W kg^{-1}. For $Ni(OH)_2$, the energy density declines sharply when the current density increases. Besides high energy density and power density, long cycle life is one of crucial factors for supercapacitors in actual applications. Fig. 7 depicts the specific capacitance as a function of cycle number at a current density of 6 A g^{-1}. The results reveal that the specific capacitance can remain at a high value of 840 F g^{-1} after 1000 cycles. We suspect that the peeling off of active materials during the fast Faradaic reaction at high current density and the erosion suffered from oxygen dissolved in the electrolyte could be responsible for the loss of capacitance during cycling.

Conclusion

In summary, we have developed a facile approach to *in situ* synthesize RGO/$Ni(OH)_2$ nanocomposites on well dispersed RGO. The introduction of RGO greatly improves the capacitance performance and rate performance of $Ni(OH)_2$. The electrodes based on RGO/$Ni(OH)_2$ nanocomposites show high specific capacitance, energy density, good rate ability and acceptable cycle stability which may lead to future potential applications in high performance supercapacitors.

Acknowledgements

This work is supported by the National Basic Research Program of China (2012CB932303) and the National Natural Science Foundation of China (Grant No. 51072215 and 51172261).

References

1 G. Wang, L. Zhang and J. Zhang, *Chem. Soc. Rev.*, 2012, **41**, 797–828.
2 C. Liu, F. Li, L.-P. Ma and H.-M. Cheng, *Adv. Mater.*, 2010, **22**, E28–E62.
3 J.-W. Lang, L.-B. Kong, W.-J. Wu, Y.-C. Luo and L. Kang, *Chem. Commun.*, 2008, 4213.
4 X. Sun, G. Wang, J.-Y. Hwang and J. Lian, *J. Mater. Chem.*, 2011, **21**, 16581.
5 D.-W. Wang, F. Li and H.-M. Cheng, *J. Power Sources*, 2008, **185**, 1563–1568.
6 H. Wang, L. Zhang, X. Tan, C. M. B. Holt, B. Zahiri, B. C. Olsen and D. Mitlin, *J. Phys. Chem. C*, 2011, **115**, 17599–17605.
7 Q. Qu, P. Zhang, B. Wang, Y. Chen, S. Tian, Y. Wu and R. Holze, *J. Phys. Chem. C*, 2009, **113**, 14020–14027.
8 C. Yuan, L. Hou, L. Yang, D. Li, L. Shen, F. Zhang and X. Zhang, *J. Mater. Chem.*, 2011, **21**, 16035.
9 J. W. Lee, J. M. Ko and J.-D. Kim, *J. Phys. Chem. C*, 2011, **115**, 19445–19454.
10 H. Jiang, T. Zhao, C. Li and J. Ma, *J. Mater. Chem.*, 2011, **21**, 3818.
11 G. M. Suppes, B. A. Deore and M. S. Freund, *Langmuir*, 2008, **24**, 1064–1069.
12 J. H. Park and O. O. Park, *J. Power Sources*, 2002, **111**, 185–190.
13 G. A. Snook, P. Kao and A. S. Best, *J. Power Sources*, 2011, **196**, 1–12.
14 M. B. Sassin, A. N. Mansour, K. A. Pettigrew, D. R. Rolison and J. W. Long, *ACS Nano*, 2010, **4**, 4505–4514.
15 S. W. Lee, J. Kim, S. Chen, P. T. Hammond and Y. Shao-Horn, *ACS Nano*, 2010, **4**, 3889–3896.
16 J. Liu, J. Sun and L. Gao, *J. Phys. Chem. C*, 2010, **114**, 19614–19620.
17 Z. Gao, J. Wang, Z. Li, W. Yang, B. Wang, M. Hou, Y. He, Q. Liu, T. Mann, P. Yang, M. Zhang and L. Liu, *Chem. Mater.*, 2011, **23**, 3509–3516.
18 X. Xia, J. Tu, Y. Mai, R. Chen, X. Wang, C. Gu and X. Zhao, *Chem.–Eur. J.*, 2011, **17**, 10898–10905.
19 H. Wang, H. S. Casalongue, Y. Liang and H. Dai, *J. Am. Chem. Soc.*, 2010, **132**, 7472–7477.
20 Q. Qu, S. Yang and X. Feng, *Adv. Mater.*, 2011, **23**, 5574–5580.
21 W. Shi, J. Zhu, D. H. Sim, Y. Y. Tay, Z. Lu, X. Zhang, Y. Sharma, M. Srinivasan, H. Zhang, H. H. Hng and Q. Yan, *J. Mater. Chem.*, 2011, **21**, 3422.
22 D. Chen, L. Tang and J. Li, *Chem. Soc. Rev.*, 2010, **39**, 3157.
23 X. Huang, X. Qi, F. Boey and H. Zhang, *Chem. Soc. Rev.*, 2012, **41**, 666–686.
24 M. Pumera, *Chem. Soc. Rev.*, 2010, **39**, 4146.
25 B. Luo, S. Liu and L. Zhi, *Small*, 2011, **8**, 630–646.
26 S. Yang, X. Wu, C. Chen, H. Dong, W. Hu and X. Wang, *Chem. Commun.*, 2012, **48**, 2773.
27 C. Xu, J. Sun and L. Gao, *J. Mater. Chem.*, 2011, **21**, 11253.

